Resistance of direct metal laser sintered Ti6Al4V alloy against growth of fatigue cracks

Resistance of Direct Metal Laser Sintered Ti6Al4V Alloy against Growth of Fatigue Cracks

R. Konečná[a], L. Kunz[b], A. Bača[c], G. Nicoletto[d]

[a]*University of Žilina, Department of Materials Engineering, Univerzitná 8215/1, 01026 Žilina, Slovakia*

[b]*Institute of Physics of Materials, Academy of Sciences of the Czech Republic, Žižkova 22, 61662 Brno, Czech Republic*

[c]*Research Centre of the University of Žilina, Univerzitná 8215/1, 01026 Žilina, Slovakia*

[d]*University of Parma, Department of Industrial Engineering, Parco Area delle Scienze, 181/A, 43100 Parma, Italy*

Abstract

Growth of long fatigue cracks in Ti6Al4V alloy prepared by selective laser melting technology was experimentally investigated. CT specimens were manufactured by direct metal laser sintering (DMLS) on EOSINT M270 system. CT specimens having three different crack orientations with respect to the DMLS build direction were manufactured with the aim to check the influence of directionality of microstructure of the DMLS material on the growth of long fatigue cracks.

It was experimentally found that there is no influence of the build orientation and related directionality of the microstructure on tensile properties, growth of long fatigue cracks and crack propagation threshold, when optimal DMLS process parameters setting is used and subsequent stress relieving heat treatment at 380 °C for 8 hours is applied on the build material.

The experimentally determined fatigue crack growth curve for Ti6Al4V manufactured by DMLS technique was compared with available literature data and with data for conventionally forged material.

The fatigue crack propagation path and fracture surfaces were investigated with

the aim to analyze the influence of the specific microstructure produced by the DMLS on the mechanism of the propagation of long cracks.

Keywords: Titanium alloys, Ti6Al4V, Fatigue crack growth, Threshold value of stress intensity factor, Direct metal laser sintering

---

1. Introduction

The rapidly developing methods of additive manufacturing (AM) over the past decade brought high expectations in industry. This technology enables the manufacture of metallic components of very complicated shape directly from the computer models [1, 2] without time consuming machining and assembly processes or preparation of casting molds. Direct metal laser sintering (DMLS) is one of the AM methods, which has a very promising potential [3, 4]. The components are built through localized melting of gas atomized powder by a concentrated laser beam. The powder is locally rapidly melted and subsequently rapidly solidified when the laser beam is moved to a neighboring area [5]. The advantage of the DMLS procedure is obvious in the development and optimization process of new components or in the case of production of small series, e.g. for biomedical applications [6, 7].

The reliable application of components produced by DMLS technology requires guaranteed mechanical properties. The static performance of many DMLS produced materials was found to be good comparable with conventionally manufactured ones [8, 9]. The problem of porosity and large defects of microstructure, which can deteriorate the tensile properties, has been in the majority of cases solved by optimization of the DMLS process parameters and the post-processing treatment, e.g. hipping [10, 11].

There is an increasing interest of industry in the production of parts, which have to fulfill severe demands on mechanical properties and high reliability also under cyclic loading. The damage tolerant design demands a knowledge of fatigue

crack growth behavior. The propagation of long cracks, particularly in the threshold region, is influenced by the material microstructure. The high number of DMLS process parameters like laser power, building layer thickness, scanning strategy etc. influences the resulting microstructure and consequently the fatigue crack growth behavior [12, 13].

Ti6Al4V is the most commonly used Ti alloy due to its outstanding engineering properties. The advantage of this alloy consists in good mechanical properties, low density and good corrosion resistance, e.g. [14, 15]. The relatively high cost, however, predetermines this material for applications with specific requirements, in aircraft industry, space technology or for manufacture of implants for human body. There are numerous studies focused on Ti6Al4V alloy manufactured by DMLS, e.g. [7, 16, 17], however, the main attention was paid to the tensile properties. The behavior under cyclic loading and particularly the fatigue crack growth resistance has been investigated in a much lower extent. The threshold stress intensity factor range of the heat treated Ti6Al4V alloy (in the 800 and 1050 °C range) for the stress ratio R = 0.1 and the crack growth perpendicular to the build direction is of about 4 $MPam^{1/2}$ [17]. The as-fabricated DMLS material exhibits a much lower value 1.4 $MPam^{1/2}$ [17]. Moreover, the threshold values were found to be slightly different for the crack growth parallel and perpendicular to the build direction. In the Paris region the crack growth rate is comparable with those determined on conventionally produced material. Moreover, a characteristic feature of as-produced DMLS alloy without heat treatment is a considerable scatter of the experimentally determined crack growth rate data for a given value of the stress intensity factor range [17, 18].

The long crack growth is influenced by material microstructure. Its effect is most pronounced in the threshold region. Investigations on the influence of microstructure on the crack growth rate and thresholds in DMLS materials indicate that there is an effect of the direction of material building [17, 19], because the

microstructure and the residual stress state are different in different directions with respect to the build direction.

This study is aimed at the experimental investigation of the growth of long fatigue cracks in Ti6Al4V alloy in different directions with respect to the DMLS build direction. The heat treatment of the alloy consisted only from the stress relieving at 380 °C/8 h in argon. The growth of long crack was studied in relation to the specific microstructure produced by the DMLS technique.

2. Experimental

2.1. Material

The specimens for tensile and fatigue crack growth testing were built from EOS titanium Ti64 alloy powder which has been optimized especially for processing on EOSINT M270 systems. Each equipment manufacturer specifies the metal powder to be used with a particular system. Powder particles used here were spherical in shape and fulfill the requirements of ISO 5832-3, ASTM F1472 and ASTM B348 standards as regards the maximum concentration of impurities. The powder particles are shown in Fig. 1a and its size distribution in Fig. 1b. The standard and real chemical compositions of the powder are listed in Table 1. The real chemical composition was determined by SEM equipped with EDX analysis.

2.2. Direct metal laser sintering process

Specimens for testing were produced on an EOSINT M270 system (EOS GmbH) directly from three-dimensional CAD design data. The system was equipped with a 200 W ytterbium fiber laser. A platform for material dispensation and a build platform were located in a build chamber filled with argon to avoid oxidation. For building of specimens the operating parameters of the system were set to laser power 200 W and the laser speed to 800 mms^{-1}. The layer thickness was 30 μm, the bead hatch distance 100 μm and the multidirectional scanning strategy of rotation between layers of the EOS DMLS system was applied. The build plate was heated to 80 °C.

2.3. Specimens

Tensile tests were conducted on flat specimens with the cross-section 4 x 6.25 mm and a gauge length 32 mm, Fig. 2. The longitudinal axes of the specimens were in three orientations in respect to the build direction; the particular types of specimens were denoted as *a*, *b* and *c*. The axis of the specimen *c* is parallel to the build direction Z. The loading axis of the specimens with orientations *a* and *b* are perpendicular to the build direction Z. The surface of the gauge length remained in the as-build state.

The specimens for fatigue crack growth determination were manufactured according to ASTM E 647-08 Standard. The characteristic specimen dimension w (i.e. distance between pin center and back surface) was 30 mm and the thickness 6 mm. The CT specimens were manufactured in such a way that the macroscopic fatigue crack growth direction was parallel to the build direction Z in orientation *a* and perpendicular to Z for the orientations *b* and *c*, Fig. 3.

Because the lateral as-build surfaces were relatively rough and not suitable for optical measurement of the crack growth, they were finely ground and carefully mechanically polished after heat treatment.

Stress relieving heat treatment is an important step in the production of parts made by DMLS. A stress relieving heat treatment at 380 °C for 8 hours was carried out in this study. The reason for this type of the heat treatment is substantiated by the idea to obtain crack growth data for the “as build” material. The heat treatment at higher temperatures which changes the material microstructure and related mechanical properties was deliberately not performed. To protect the surface from oxidization, the heat-treatment was conducted in argon atmosphere.

2.4. Mechanical testing, investigation of microstructure, fractography

A servohydraulic testing machine MTS 810 with an extensometer having 25

mm gauge length was used for experimental determination of the tensile properties. Test methods fulfilled the ASTM 8/E 8M-08 Standard. The loading rate was 0.01 mms^{-1}.

The fatigue crack growth testing was conducted under load control on a Roell/Amsler HFP 5100 resonant testing machine. The loading asymmetry characterized by the ratio R (minimum to maximum load in a loading cycle) was 0.1. The loading frequency was in the interval 80 - 50 Hz and was dependent on the crack length, i.e. on the stiffness of the specimen. Both the tensile tests and the fatigue crack growth measurement were performed at ambient laboratory conditions.

The length of the fatigue crack was optically measured on both lateral sides of specimens by means of two CCD cameras situated on travelling supports. The crack length was determined with the 0.01 mm accuracy.

The load shedding procedure was used after the crack initiated from the starting notch. The load amplitude was reduced at the constant R ratio in such a way that the crack growth rate of the order of 10^{-7} mm/cycle was reached. The determination of the crack growth rates was carried out at the constant load amplitude and fulfilled the requirements of the ASTM E647-08 Standard.

The microstructure produced by DMLS on three metallographic sections of each specimen was observed with a light microscope Zeiss Axio Observer Z1M after conventional preparation and etching (i.e. 10% HF). The fracture surfaces were studied in a scanning electron microscope Tescan LYRA 3 XMH FEG/SEM. The determination of the fracture roughness profiles in the threshold and in the Paris regions were optically measured using image analysis software.

3. Results

Fig. 4 shows an example of the stress-strain curves obtained by tensile tests on three specimens with different mutual orientations of the build direction and loading direction. The build orientation influences slightly the tensile properties, see Table 2. The ultimate tensile strength σ_{UTS} of the specimens with the orientations *a* and *b*, is

1255 ± 21 and 1235 ± 11 MPa respectively and the error scatterbands are overlapping. The σ_{UTS} of specimens with orientation *c*, i.e. the loading axis is perpendicular to the build layers, is lower, namely 1195 ± 9 MPa. Similarly small is the influence of the orientation on the yield stress $\sigma_{0.2}$ and the elongation to rupture.

The experimentally determined fatigue crack growth rate dependence on the stress intensity factor range ΔK is shown in Fig. 5. The data exhibit a large scatter. Nevertheless, there is no detectable influence of crack direction with respect to build orientation on the crack propagation rate and on the crack propagation threshold. With decreasing ΔK the crack rate decreases and tends to reach the threshold value ΔK_{th} = 3.7 $MPam^{1/2}$. The crack growth rate in dependence on the stress intensity factor range ΔK can be generally described by the equation [20]

$$da/dN = A(\Delta K^{m} - \Delta K_{th}^{m}). \quad (1)$$

Taking into account the threshold value 3.7 $MPam^{1/2}$, the experimental points can be well approximated by the equation

$$da/dN = 3 \times 10^{-8} \Delta K^{3.0} - 1.52 \times 10^{-6}, \quad (2)$$

which is shown in Fig. 5 by the full line.

Observation of microstructure on three mutually perpendicular planes was made both for tensile and CT specimens. The microstructure of tensile and CT specimens is identical and exhibits some degree of directionality. The microstructure on z-x and z-y (lateral) planes that are parallel to the build direction, Fig. 6a, is characterized by primary columnar β grains, which transformed during cooling to fine needles of α'-martensite, Fig. 6b and Fig. 7b. This type of microstructure corresponds to the microstructure typical of as-fabricated products [21, 22]. The temperature of the stress relieving heat treatment (380 °C/8 h) was too low to transform the original microstructure. The elongated β grains having the length of several building layers grew in the build direction and exhibit a texture. Black spots on the optical micrograph, Fig. 6a, correspond to the regions of locally substantially finer microstructure. These regions are elongated in the direction perpendicular to the

build direction. The finer microstructure is a consequence of high local internal thermal gradients and high cooling rates caused by the laser beam passes. Moreover, elongated microshrinkages with sharp edges were locally present in the black spots. The microstructure, Fig. 7, observed on the horizontal plane (x-y) perpendicular to the build direction shows different features when compared to the lateral planes. Fig. 7a shows polyhedral grains corresponding to the perpendicular sections of columnar primary β grains. The size of these grains is defined by the width of the columnar grains.

The fatigue cracks propagate in DMLS produced material in a transgranular way. Examples of fatigue fracture surface profiles of the specimen *c* together with the microstructure are shown in Fig. 8. The transgranular character of the crack propagation was observed both for the threshold region, Fig. 8a, where the crack rate is low and also for the Paris region, Fig. 8b. The propagating crack does not interact with the grain boundaries of prior β phase. The propagation takes place by damaging of the very fine needle structure of acicular α′-martensite at the crack tip. The fracture profiles are flat with local small sharp asperities. No significant difference in the fatigue fracture surface profiles was found for the three specimen orientations *a*, *b* and *c*.

The typical fracture surface appearance does not change significantly with increasing crack propagation rate from the threshold region up to the crack rate of the order 1 x 10^{-4} mm/cycle. Fig. 9 brings an example of the fracture surface of the specimen *c*. The observed independence of the fracture surface appearance on the fatigue crack rate is in accordance with the independence of the fracture surface roughness Ra on the crack growth rate (Ra is the arithmetic average of the absolute roughness profile). The Ra values for three types of specimens *a*, *b* and *c* in the threshold region and in Paris region are given in Table 3. It can be seen that there is no substantial difference among the Ra for orientation *a* and *b* and there is also no substantial difference of fracture surface profile roughness in threshold and Paris region. The roughness of the fracture surface corresponding to the specimen *c* seems to be also independent on

the crack growth rate, however it is higher than that of specimens *a* and *b*. The difference in the surface roughness can be explained by the fact that the fatigue crack propagates parallel to the building layers in the specimen *c*, whereas it propagates across the layers in the specimens *a* and *b*.

3. Discussion

The tensile properties are only very weakly dependent on the build orientation, i.e. on the directionality of microstructure. Somewhat higher are both the σ_{UTS} and $\sigma_{0.2}$ for the orientation when the loading is applied parallel to the build layers and marginally worse when the loading is perpendicular to the build layers. The explanation may be based on the influence of small and rare microshrinkages elongated in the building plane. The inherent α′-martensite fine needle microstructure, Figs. 6b and 7b, does not exhibit any specific directionality. The tensile properties are good comparable with those of conventionally manufactured alloy heated for 1 h at 1050 °C and quenched in water, as it can be seen from Fig. 4, where comparison with tensile curve published by Fan et al. [23] is shown. The presented microstructures of DMLS after stress relieving treatment and conventionally prepared material after heat treatment with martensitic structure are comparable.

The experimental points presented in Fig. 5 correspond to the crack growth measurement performed solely under constant load amplitude, i.e. under increasing ΔK. This is a difference to the data published by the present authors in [24], where the experimental points were collected both under increasing ΔK and also decreasing ΔK (load shedding procedure). The data scatter in Fig. 5 in this work is somewhat lower than the scatter of experimental points in [24]. Note that the data determined under decreasing load conditions were valid according to the ASTM E647-08 Standard. The values of m and A parameters in eq. (1) fitted to the data corresponding to the constant amplitude loading are only marginally different from

that published in [24]. Similar conclusion can be made as regards the threshold value ΔK_{th}. The small difference in the crack growth rate scatter for measurement covering both the constant and decreasing loading may indicate high sensitivity of the DMLS material to the changes of loading conditions.

The crack growth data for as-fabricated DMLS Ti6Al4V alloy published by Becker et al. [18] are replotted together with our data in Fig. 10. The crack growth measurement was performed on CT specimens with characteristic dimension w = 25 mm and the thickness of one half of the specimens used in this study. For low ΔK values the crack rates are two orders of magnitude higher than the rates determined in this work for a DMLS Ti6Al4V stress relieved at 380 °C for 8 hours. The scatter of the experimental points in both cases is high. In the case of the as-fabricated alloy investigated in [18] the authors express the idea that the large scatter may be attributed to the residual stresses present in specimens. Occurrence of non-uniform residual stresses approaching the yield stress in as-fabricated DMLS Ti6Al4V alloy was reported in [25]. In this work, however, the heat treatment applied to CT specimens resulted in full stress relieving, which was proved by X-ray measurements prior to testing. Only insignificant residual compressive stresses not exceeding 30 MPa were detected. This indicates, that the scatter is more likely related to the non-continuous crack growth observed on the specimen surface. This effect is similar for all three crack growth directions, without any relevance to the build direction. The large data scatter in the case on as-build material is evident also from the paper by Leuders et al. [17] where, however, direct current potential drop was used for the crack monitoring. This method should eliminate the problems with locally different crack growth rate along the crack front, which can manifest itself in the case of optical surface crack increment monitoring.

Low temperature stress relieving and annealing heat treatments improve fatigue crack growth resistance relative to the as-build condition and eliminate the influence of anisotropy [26]. Fig. 10 shows comparison of the crack growth curve determined in this work with results on as-build material by Leuders et al. [17] for

two orientations *a* and *c*. It is obvious from the comparison that (i) the stress relieving used in this study improves the threshold behavior and (ii) removes the effect of directionality. It is worthwhile to note that the stress reliving in our case did not change noticeably the as-build microstructure.

The fatigue crack growth rates of the present study and the data replotted from paper by Cain et al. [26] are shown in Fig. 10. Inspection of the figure reveals that all specimens of both studies show very similar behavior and actually overlap when in the same ΔK range. It can be concluded that all data from the crack growth threshold up to the rates of the order 10^{-3} mm/cycle can be described by the eq. (2).

The fatigue crack propagates in a transgranular mode through the very fine structure consisting of needles of α'-martensite, which was transformed from the prior columnar β grains during rapid cooling in the DLMS process. The original boundaries of columnar β grains do not obviously influence the crack paths, as it can be concluded from Fig. 8a, which shows the growth of the crack across the build layers. The fracture surface appearance is very similar in the whole measured range of the crack growth rates. From fracture surface observations it follows that the damage of the fine structure consisting of needles of α'-martensite at the tip of the fatigue crack is the decisive process of the crack propagation. The measurement of fracture surface roughness evidenced higher values for the fracture surface created by the crack propagation along the layers when compared to the propagation across the layers but this fact seems to be not decisive for the crack growth. The directionality of the prior columnar β grains does not play a role, i.e. the resistance of the material against the crack growth is the same in the case when the crack intersects the build layers, (specimens *a* and *b*) or propagates along the layers, specimen *c*.

The applied parameters of the DMLS process resulted in an alloy which has homogeneous microstructure in the scale of tens of microns, compare Figs. 6b and 7b. The directionality of structure, which appears at lower magnification and irregularities related with dark areas and locally finer microstructure, Fig. 6a have no significant effect on the long crack growth. In the frame of the large data scatter,

which seems to be inherent to the material behavior in as-build condition, there is no apparent influence of the building orientation on the crack propagation rate and on the crack propagation threshold $\Delta K_{th,}$ which is equal to 3.7 $MPam^{1/2}$.

Fig. 11 shows the comparison of the experimentally determined crack growth curve from Fig. 5 (black line, eq. (2)) with literature data on conventionally produced Ti6Al4V alloy. It can be seen that in the Paris region the crack growth resistance of the DMLS alloy is fully comparable with the alloy produced conventionally. The threshold value 3.7 $MPam^{1/2}$ is lying in the range from 3 to 5 $MPam^{1/2}$ of conventional material which follows from papers [27-29]. Based on the present study it can be concluded that the long fatigue crack growth resistance of the Ti6Al4V alloy prepared by DMLS technology is fully comparable with the material prepared conventionally.

4. Conclusions

The growth of long fatigue cracks in Ti6Al4V alloy manufactured by direct metal laser sintering and subsequent stress relieving at 380 °C/8 h can be described for loading conditions with stress ratio R = 0.1 by the equation

$$da/dN\ [mm/cycle] = 3 \times 10^{-8}\ \Delta K^{3.0} - 1.52 \times 10^{-6}.$$

The equation covers a broad range of growth rates from threshold ΔK_{th} = 3.7 $MPam^{1/2}$ up to the rates of the order 10^{-3} mm/cycle.

The studied Ti6Al4V alloy does not exhibit dependence of the tensile properties and long crack growth on the build direction.

The crack growth data have large scatter which is characteristic feature of the as-fabricated material. It was found that the scatter is not related to the residual stresses which are in some studies believed to be the cause of this phenomenon. The observed scatter is more likely related to the non-continuous crack growth observed on the specimen surface.

The crack growth rates and the crack propagation threshold are comparable with those determined for conventionally manufactured alloys.

Fatigue crack growth takes place in a transgranular mode by cyclic damaging of acicular α'-martensite within the plastic zone. The original β grain boundaries do not play an important role in the crack growth process.

Acknowledgment

The research was supported by project VEGA grant No. 1/0196/12 and European project Research Centre of the University of Žilina - Second Phase: ITMS 26220220183. The company BEAM-IT, Fornovo Taro, Italy is gratefully acknowledged for specimen production.

References

[1] M. Agarwala, D. Bourell, J. Beaman, H. Marcus, J. Barlow, Direct selective laser sintering of metals, Rapid Prototyping Journal, 1 (1995) 26-36.

[2] J. P. Kruth, P. Mercelis, J. V. Vaerenbergh, L. Froyen, M. Rombouts, Binding mechanisms in selective laser sintering and selective laser melting, Rapid Prototyping Journal, 11 (2005) 26-36.

[3] G. Levy, R. Schindel, J. P. Kruth, Rapid manufacturing and rapid tooling with layer manufacturing (LM) technologies, state of the art and future perspectives. CIRP Annals-Manufacturing Technology, 52(2) (2003) 589-609.

[4] I. Gibson, D. W. Rosen, B. Stucker, Additive manufacturing technologies: Rapid prototyping to direct digital manufacturing. New York: Springer, 2010.

[5] K. Antony, N. Arivazhagan, Studies on energy penetration and marangoni effect during laser melting process, Journal of Engineering Science and Technology, 10(4) (2015) 509-525.

[6] L. E. Murr, E. Martinez, K. N. Amato, S. M. Gaytan, J. Hernandez, D. A. Ramirez, R. B. Wicker, Fabrication of metal and alloy components by additive manufacturing: Examples of 3D materials science, Journal of Materials Research and Technology, 1(1) (2012) 42-54.

[7] B. Vandenbroucke, J. P. Kruth, Selective laser melting of biocompatible metals for rapid manufacturing of medical parts, Rapid Prototyping Journal, 13(4) (2007) 196-203.

[8] G. D. Kim, Y. T. Oh, A benchmark study on rapid prototyping processes and machines: Quantitative comparisons of mechanical properties, accuracy, roughness, speed, and material cost, Proceedings of the Institution of Mechanical Engineers Part B Journal of Engineering Manufacture 222(2) (2008) 201-215.

[9] T. M. Mower, M. J. Long, Mechanical behavior of additive manufactured, powder-bed laser-fused materials. Mater. Sci. Eng. A 651, (2016) 198-213.

[10] M. Shellabear, O. Nyrhilä, DMLS - development history and state of the art, in: Proceedings of the 4th International Conference on Laser Assisted Net Shape Engineering, LANE 2004, Erlangen, Germany, (2004) 393-404.

[11] H. Gong, K. Rafi , T. Starr, B. Stucker, The effects of processing parameters on defect regularity in Ti-6Al-4V parts fabricated by selective laser melting and electron beam melting, 24th Annual International Solid Freeform Fabrication Symposium (2013) 424-439.

[12] I. Gibson, D. P. Shi, Material properties and fabrication parameters in selective laser sintering process, Rapid Prototyping Journal, 3(4) (1997) 129-136.

[13] M. Krishnan , E. Atzeni, R. Canali , F. Calignano, D. Manfredi, E. P. Ambrosio, L. Iuliano, On the effect of process parameters on properties of AlSi10Mg parts produced by DMLS, Rapid Prototyping Journal, 20(6) (2014) 449-458.

[14] M. Donachie, Titanium, A technical guide, 2nd edition. ASM international, 2000.

[15] C. Leyens, M. Peters, Titanium and titanium alloys - Fundamentals and applications, Wiley-VCH GmbH & Co. KGaA, 2003.

[16] T. Vilaro, C. Colin, J. D. Bartout, As-fabricated and heat-treated microstructures of the Ti-6Al-4V alloy processed by selective laser melting, Met. Mat. Trans 42A

(2011) 3190-3199.

[17] S. Leuders, M. Thöne, A. Riemer, T. Niendorf, T. Tröster, H. A. Richard, H. J. Maier, On the mechanical behaviour of titanium alloy TiAl6V4 manufactured by selective laser melting: Fatigue resistance and crack growth performance, International Journal of Fatigue, 48 (2013) 300-307.

[18] T. H. Becker, M. Beck, C. Scheffer, Microstructure and mechanical properties of direct metal laser sintered Ti-6Al-4V. South African Journal of Industrial Engineering 26 (2015) 1-10.

[19] A. Riemer, H. A. Richard, J. P. Brüggemann, J. N. Wesendahl, Fatgiue crack growth in additive manufactured products. Frattura ed Integrità Strutturale 34 (2015) 437- 446.

[20] M. Klesnil, P. Lukáš, Fatigue of Metallic Materials, Elsevier, Amsterdam 1992.

[21] B. Vrancken, L. Thijs, J. P. Kruth, J. Humbeeck, Heat treatment of Ti-6Al-4V produced by selective laser melting: Microstructure and mechanical properties, Journal of Alloys and Compounds, 541 (2012) 177-185.

[22] M. Simonelli, Y. Y. Tse, C. Tuck, Further understanding of Ti6Al4V selective laser melting using texture analysis, 23rd Annual International Solid Freeform Fabrication Symposium: An Additive Manufacturing Conference, Proceedings, August 6-8, Solid freeform fabrication proceedings, (2012) 480-491, ISSN 1053-2153.

[23] Y. Fan, W. Tian, Y. Guo, Z. Sun, and J. Xu, Relationships among the microstructure, mechanical properties and fatigue behavior in thin Ti6Al4V, Advances in Materials Science and Engineering 2016, Article ID 7278267, http://dx.doi.org/10.1155/2016/7278267.

[24] R. Konečná, L. Kunz, A. Bača, G. Nicoletto. Long fatigue crack growth in Ti6Al4V produced by direct metal laser Sintering, Procedia Engineering 160 (2016) 69-76.

[25] C. R. Knowles, T. H. Becker, R. B. Tait, Residual stress measurements and structural integrity implications for selective laser melted Ti-6Al-4V, South African Journal of Industrial Engineering, 23 (2012) 119-129.

[26] V. Cain, L. Thijs, J. Van Humbeeck, B. Van Hooreweder, R. Knutsen, Crack propagation and fracture toughness of Ti6Al4V alloy produced by selective laser melting, Additive Manufacturing 5 (2015) 68-76.

[27] B. L. Boyce, R. O. Ritchie, Effect of load ratio and maximum stress intensity on the fatigue threshold in Ti-6Al-4V. Engineering Fracture Mechanics 68 (2001) 129-147.

[28] Y. Okazaki, Comparison of fatigue properties and fatigue crack growth rates of various implantable metals. Materials 5 (2012) 2981-3005.

[29] H. Oguma, T. Nakamura, Fatigue crack propagation properties of Ti–6Al–4V in vacuum environments, International Journal of Fatigue 50 (2013) 89-93.

	Al	V	O	N	H	Fe	C	Ti
standard value	5.5 - 6.5	3.5 - 4.5	< 0.100	< 0.050	< 0.012	< 0.250	< 0.080	balance
real value	6.06	3.90	0.085	0.006	0.002	0.250	0.007	balance

Table 1. Chemical composition of Ti6Al4V powder in wt. %.

orientation	σ_{UTS} [MPa]	$\sigma_{0.2}$ [MPa]	A [%]
a	1255 ± 21	968 ± 14	5.4 ± 0.5
b	1235 ± 11	957 ± 4	6.5 ± 0.6
c	1195 ± 9	952 ± 1	7.4 ± 1.2

Table 2. Tensile properties of DMLS specimens with different orientation to the build direction.

	specimen *a* threshold region	specimen *a* Paris region	specimen *b* threshold region	specimen *b* Paris region	specimen *c* threshold region	specimen *a* Paris region
Ra [μm]	7.06	5.47	6.11	4.70	10.4	12.4

Table 3. Fatigue fracture surface roughness in threshold and Paris region.

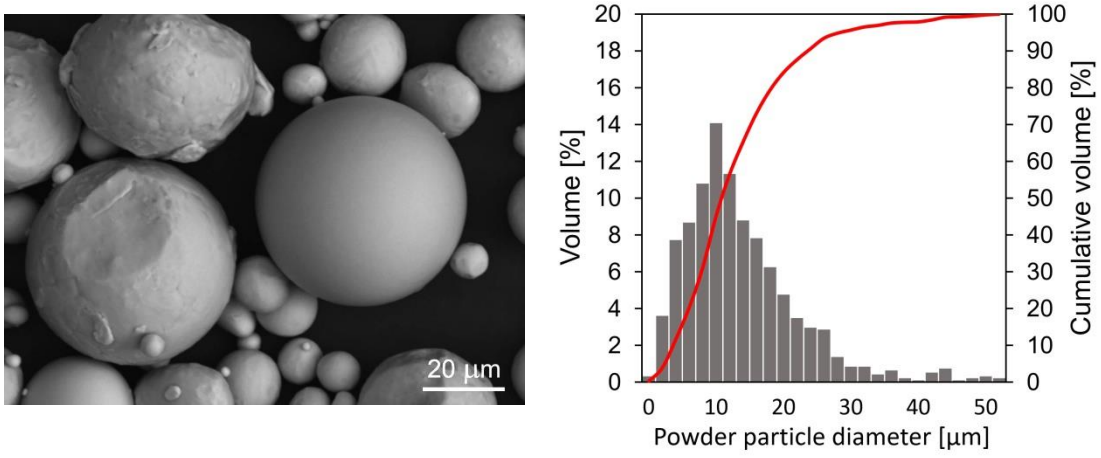

a) b)

Fig. 1. a) Ti6Al4V powder particles used for production of specimens. b) Powder particle size distribution.

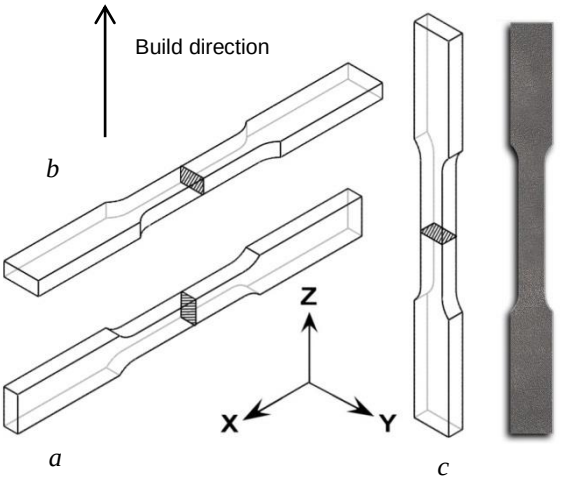

Fig. 2. Three orientations of specimens for tensile test with respect to the build direction. The cross-section plane for the orientations *a* and *b* is the plane z-y and for *c* x-y.

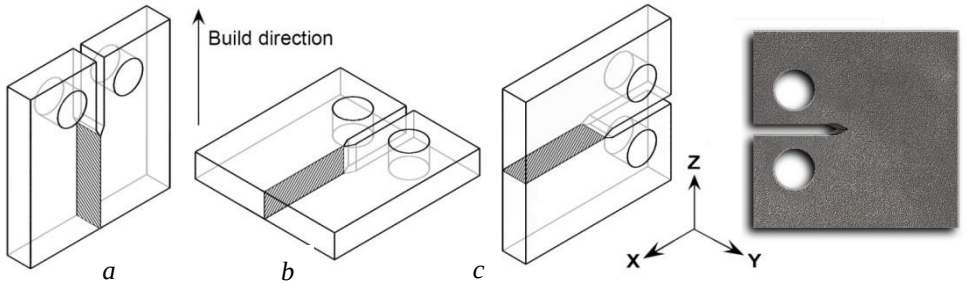

Fig. 3. Three orientations of CT specimens for crack growth tests with respect to the build direction Z, the macroscopic crack plane for the orientation *a* coincides with the plane z-y, *b* with plane z-x and *c* with plane x-y.

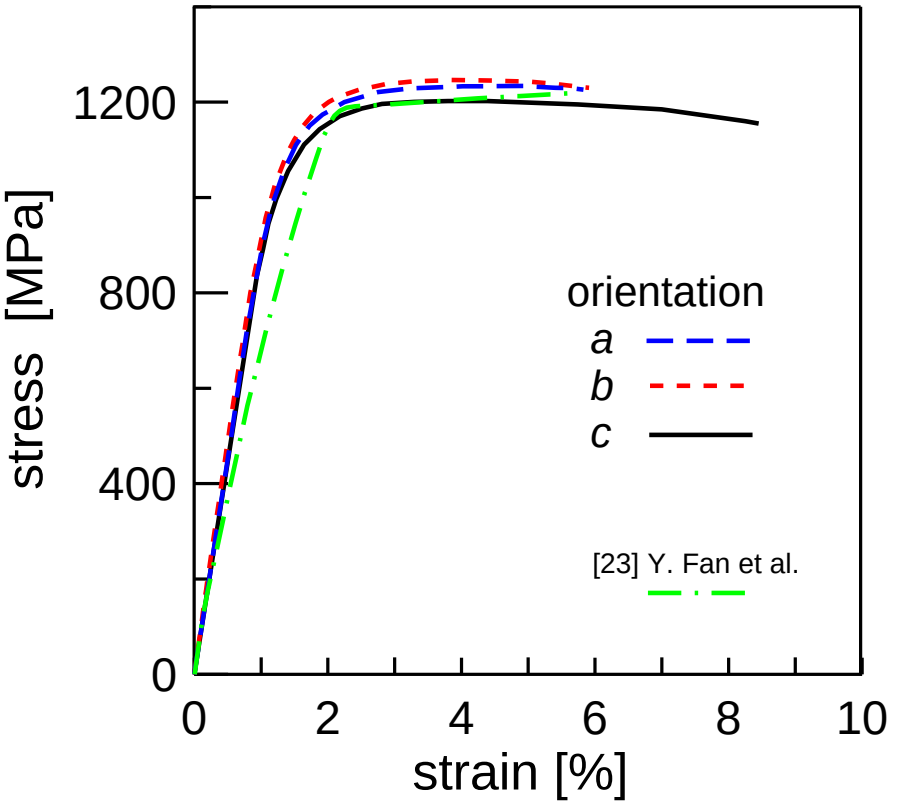

Fig. 4. Stress-strain curves of DMLS and conventional Ti6Al4V alloy.

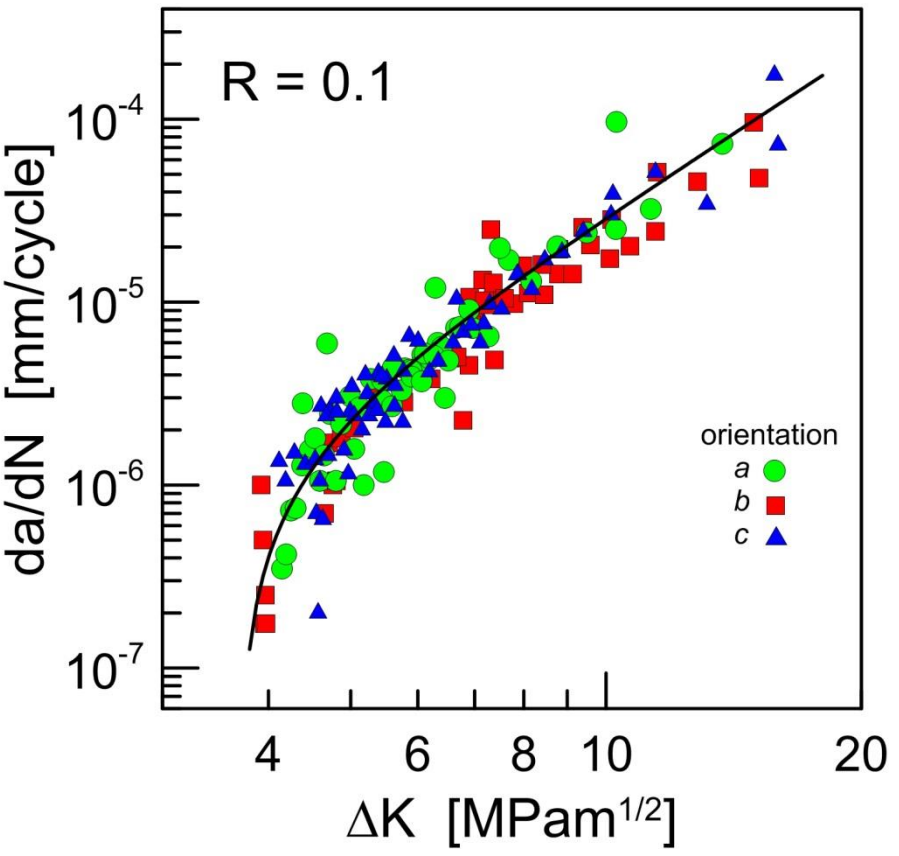

Fig. 5. Fatigue crack growth data for Ti6Al4V alloy manufactured by DMLS.

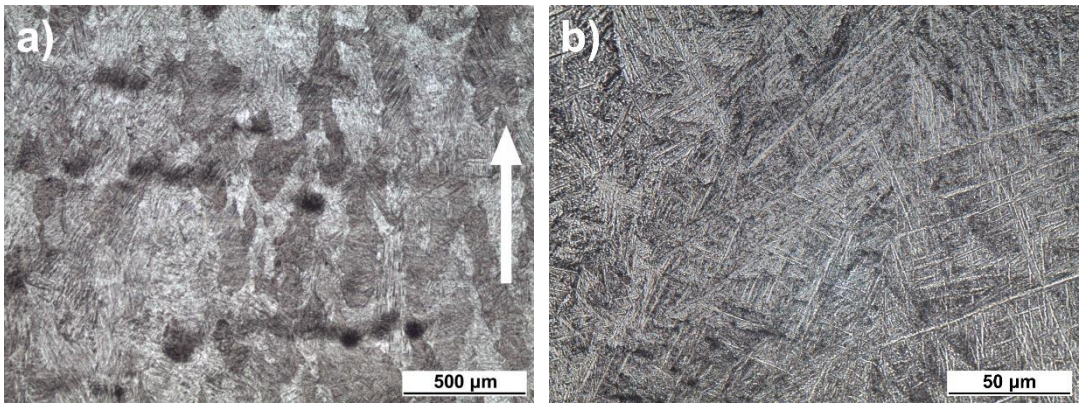

Fig. 6. Microstructure a) as revealed on the lateral planes, b) details of α'-martensite fine needles, etched by 10% HF. Build direction is indicated by the arrow.

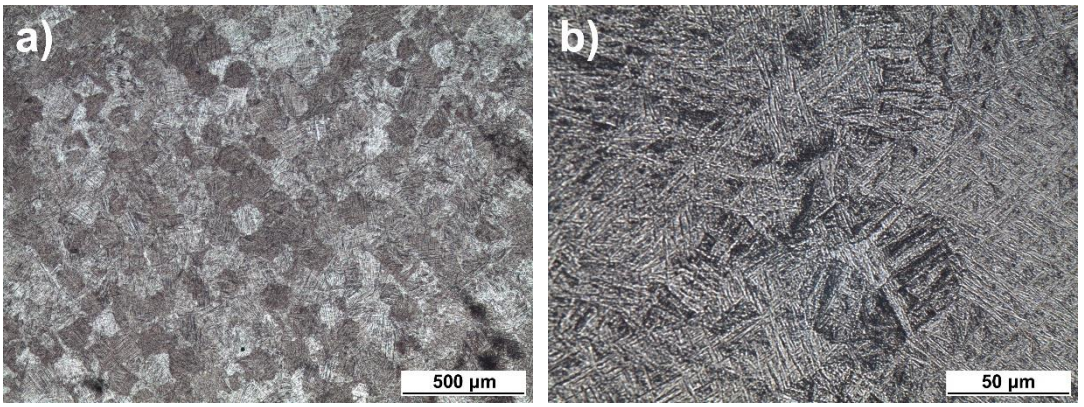

Fig. 7. Microstructure a) as revealed on the horizontal plane and b) details of α'-martensite fine needles, etched by 10% HF. Build direction is perpendicular to the observed surface.

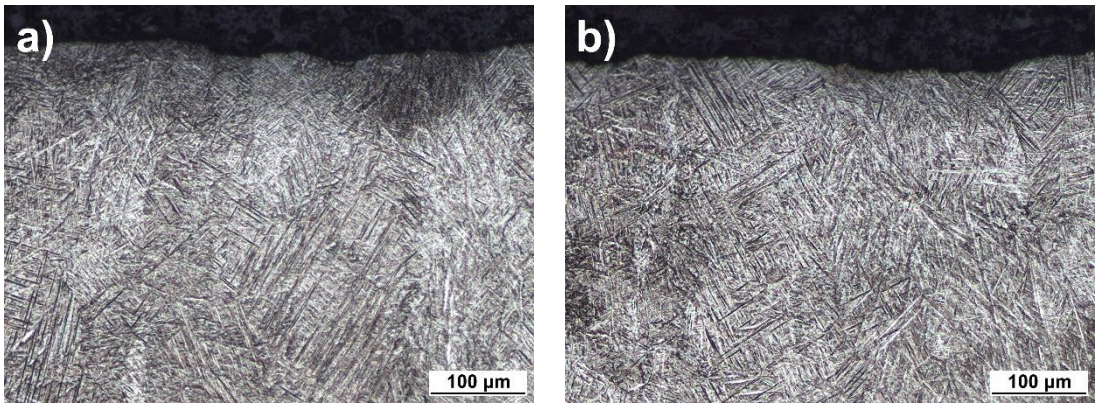

Fig. 8. Fatigue facture surface profiles, a) threshold region, da/dN ~ 10^{-7} mm/cycle, specimen orientation *c*. b) Paris region, da/dN ~ 10^{-5} mm/cycle, specimen orientation *c*, etched by 10% HF. The build orientation is perpendicular to the fracture surface.

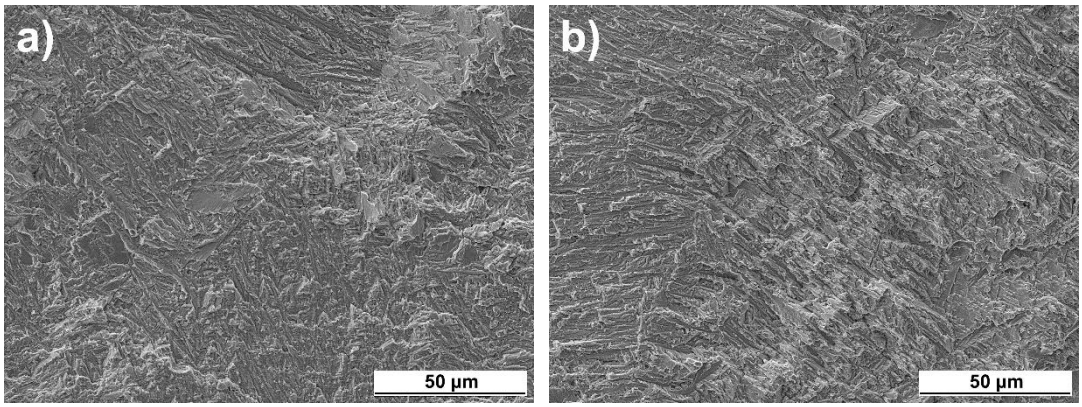

Fig. 9. Examples of fatigue fracture surfaces of specimen c, a) threshold region, da/dN ~ 10^{-7} mm/cycle, b) Paris region, da/dN ~ 10^{-5} mm/cycle.

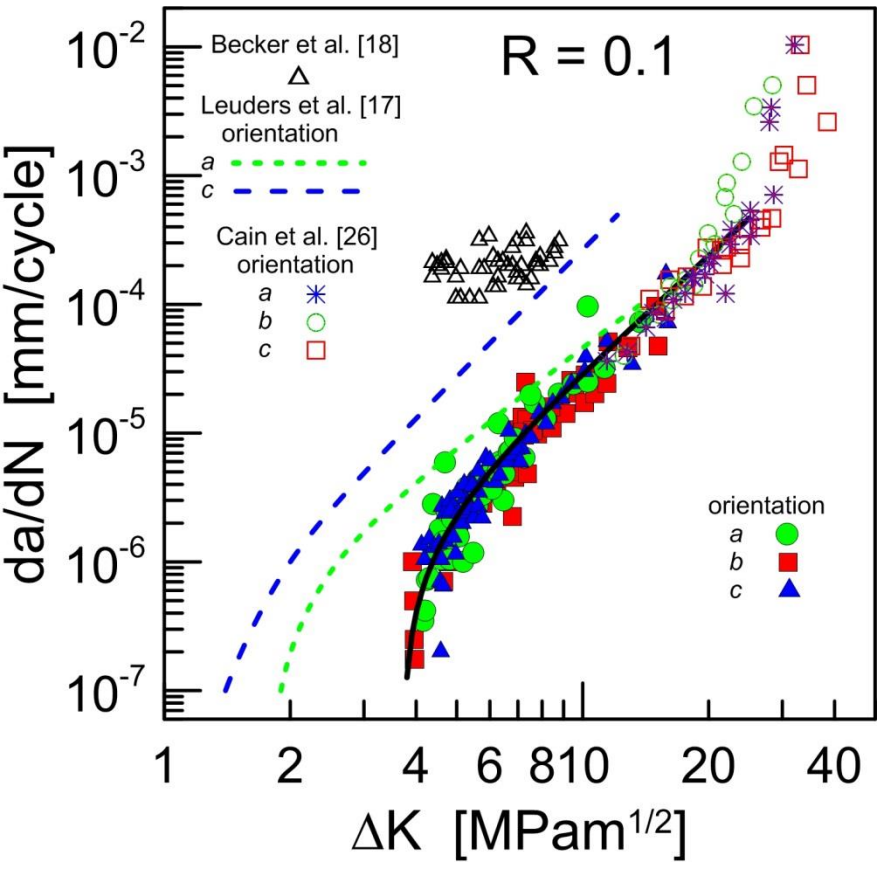

Fig. 10. Fatigue crack growth curves for as build and heat treated Ti6Al4V alloy produced by DMLS.

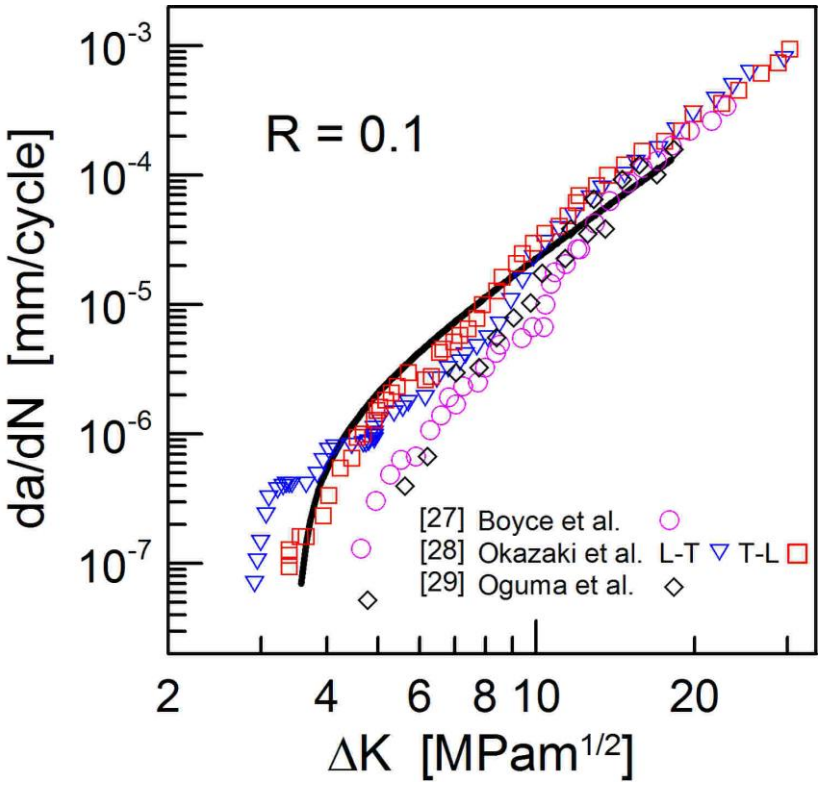

Fig. 11. Comparison of fatigue crack growth rates in Ti6Al4V prepared by DLMS (black continuous line) and conventionally (different symbols).